Kovove Mater. 50 2012 433–440
DOI: 10.4149/km_2012_6_433

Microstructure and texture evolution during ECAP of pure aluminium and Al-4vol.%Al_4C_3 powder alloy

M. Orolínová[1]*, J. Ďurišin[1], M. Besterci[1], K. Ďurišinová[1], R. Kočiško[2], T. Kvačkaj[2], K. Saksl[1], Z. Orolínová[3]

[1] *Institute of Materials Research, Slovak Academy of Sciences, Watsonova 47, 040 01 Košice, Slovak Republic*
[2] *Department of Metals Forming, Faculty of Metallurgy, Technical University, Vysokoškolská 4, 04 200 Košice, Slovak Republic*
[3] *Institute of Geotechnics of the Slovak Academy of Sciences, Watsonova 45, 043 53 Košice, Slovak Republic*

Received 23 March 2012, received in revised form 31 May 2012, accepted 17 September 2012

Abstract

The study is focused on the microstructure and texture evolution in pure aluminium (prepared by the conventional casting technology) in comparison with the dispersion strengthened system Al-4vol.%Al_4C_3 (prepared by the powder metallurgy method) during the ECAP deformation. The ECAP process of the pure aluminium led to the dislocation cell and subsequent subgrain structure formation with a mean subgrain of 2 μm. An application of ECAP method in the powdered alloy led to the transversal fragmentation of as-received elongated grains and mainly nanosized grains formation. The final size of the grains was approximately 100 nm.

Pure aluminium after the ECAP contained a similar, but stronger, crystal orientation as-received Al (200) and in addition Al (311) orientation. In composite aluminium material the as-received Al (111) after the ECAP evolved into the dominating crystal orientation Al (220).

K e y w o r d s: aluminium, dispersion strengthened Al, microstructure, texture, ECAP

1. Introduction

Submicrocrystalline materials have recently stimulated considerable interest among researchers [1]. These materials are characterized by a very fine grain size and a large amount of grain boundary area what results in their very attractive properties. Many technologies are available to produce ultra fine grain size, but they are unable to be used for the production of large bulk samples [2–5]. For this reason, much attention has been given to techniques using severe plastic deformation (SPD). Various SPD methods have been developed to produce a wide range of ultra-fine and nano-scale grained metals and alloys [6–8]. The most popular SPD technique is so-called equal-channel angular pressing (ECAP) suitable to cost effective production of the ultrafine-grained materials in bulk form [9, 10]. In processing by ECAP a sample is deformed in a narrow deformation zone at the plane of an intersection of two die channels whose cross sections are of equal areas and the strain mode approximates closely to simple shear. As the overall billet geometry remains nearly constant during the ECAP, multiple passes and different routes are possible without any reduction in cross-sectional area. This allows the materials to be deformed at very high plastic strain that cannot be readily obtained via the more conventional manufacturing processes, such as rolling or extrusion [11]. Usually, in dependence on the applied deformation methods (processing conditions), when different strain (von Mises) at deformation is developed, various structures of the deformed materials can be found [12, 13].

Many researchers consider that the structure evolution during the SPD processing broadly follows classic mechanisms and concept of structural changes occurring during the conventional processes. During the plastic deformation at low temperatures a new high angle boundary area can be generated by two main mechanisms that operate simultaneously: an extension of pre-existing boundaries and generation of new

*Corresponding author: tel.: +421/55/7922467; fax: +421/55/7922408; e-mail address: morolinova@imr.saske.sk

high angle boundaries formed by the grains subdividing. More recent studies have suggested that grain refinement in pure aluminium is dependent also on the precise purity level of the material [14, 15]. Grain refinement during the SPD is significantly influenced by the presence of non-shearable particles in the alloy [16]. These particles markedly influence the thermal stability of the microstructure after the ECAP, too [17]. The SPD process was followed by the formation of high-angle grain boundaries characterized by various orientation vectors as well as developed crystallographic texture [18], and the texture evolution was modelled in several works [19–21]. The deformation occurring in ideal ECAP conditions may be approximated by simple shear along a single plane crossing the ECAP channel [22]. Polycrystalline materials respond to the macroscopic shear stress by deformation of individual grains through movement of dislocations on one or more of the properly oriented crystallographic slip planes, combined with the rotation of grains, the main crystallographic slip planes slew to the direction parallel to the macroscopic shear direction.

Several factors (flow strength on the slip systems, resistance to grain rotation, grain size) influence these processes. It is known that the crystallographic texture of metals reflects most microstructural changes that occurred during the deformation process. It has been reasonably speculated that the extent of the ultimate grain refinement probably depends, at least in part, on the interaction of the shear plane in each separate pressing operation with the induced texture and the crystal structure of the material [22]. Accordingly, measurements of the texture evolution during ECAP are an important requirement for development and detailed understanding of the grain refinement process. The influence of ECAP processing parameters on the microstructural and/or texture development using the sample of the pure Al and/or Al alloy was investigated in several reports [21, 23, 24].

In this study, the microstructure and texture evolution during the ECAP process of the aluminium materials was investigated. The paper is aimed at the comparison of the microstructural and textural changes during the ECAP process of the conventionally prepared pure aluminium and the dispersion strengthened Al-4vol.%Al_4C_3 alloys prepared by the powder metallurgy.

2. Experimental materials and methods

The experiments were conducted on the pure aluminium and the Al-4vol.%Al_4C_3 material. The commercial aluminium of 99.9 % purity was prepared by the conventional casting technology. The experimental sample before the ECAP pressing (as-received) had a bar form with diameter $\varnothing = 10$ mm and length $l = 80$ mm. The dispersion strengthened system of Al-4vol.%Al_4C_3 was prepared by the powder metallurgy method – mechanical alloying. Low-oxygen Al powder with the powder particle size < 50 μm was dry milled in an attritor for 90 min with the corresponding amount of graphite KS 2.5 creating 4 vol.% Al_4C_3. The attrition milling parameters: rotating speed 900 r min^{-1}, ball to powder ratio 4 : 0.15. The graphite particles were rapidly fragmentated during the milling due to their excellent cleavage. In the process of high energy milling the uniform distribution of graphite occurred, hereby its particular transformation to carbide as well as refining of the Al matrix was observed. Then the specimen was cold pressed using a load of 600 MPa. The cylindrical shape of the specimen was obtained. Subsequent heat treatment at 823 K for 3 h induced the chemical reaction: $4Al + 3C \rightarrow Al_4C_3$. The complete transformation of graphite to carbide occurred at these conditions of heat treatment in accordance with the kinetic curves of the carbidization [25]. The cylinder was next hot extruded at 873 K with 94 % reduction of the cross section (as-received). The samples of the pure and dispersion strengthened aluminium were extruded at the ambient temperature in the ECAP machine [26] using processing route C, in which the sample rotated by 180° in the same directions between the consecutive passes. Because these different materials show of course different deformation ability, the total number of ECAP passes of the pure aluminium sample and the Al-Al_4C_3 material was 8 and 2, respectively. Due to the complex deformation mode operating in the process, there was a gradient existing from the top to the bottom part of the ECAP-deformed billet. Consequently, the microstructure and texture formation were non-uniform across the billet. This was also shown for copper and aluminium alloy [27]. Therefore, all cuttings for the sample extraction were done in the same way. Measurements were performed on the cross section.

The microstructures of the as-received and as-processed materials were observed by transmission electron microscope (TEM) Philips CM 20 using the foil method. The grain size was determined by direct measuring of about 100 grains in thin foils. The Al_4C_3 particle size was determined by measuring of about 200 particles.

The qualitative phase analyses and texture were performed using the X-ray diffraction methods. The X-ray diffraction patterns were obtained by Philips X'Pert Pro powder diffractometer equipped with Ni-filtered Cu Kα radiation using the positional sensitive detector X'Celerator. Qualitative phase analyses were determined using the High Score program and PDF 2 (Powder Diffraction File). Texture of experimental materials was analysed by texture coefficients. The texture coefficients characterizing the preferred orientation of the materials were calculated from the

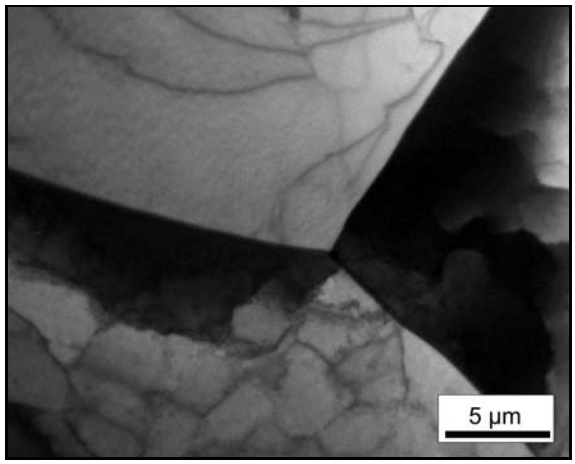

Fig. 1. TEM microstructure of as-received pure aluminium.

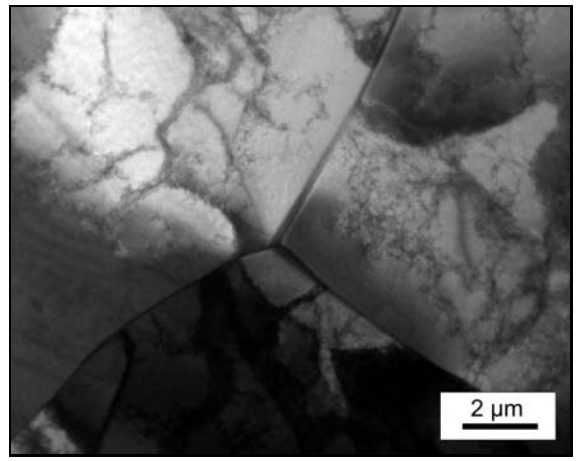

Fig. 2. TEM microstructure of pure aluminium after two ECAP passes.

X-ray diffraction data using the Harris method [28]:

$$\mathrm{TC}_{hkl} = \frac{I_{hkl}/I_{0hkl}}{1/n \sum_{i=1}^{n} (I_{hkl}/I_{0hkl})}, \qquad (1)$$

where TC_{hkl} is the texture coefficient of the reflection (hkl), I_{hkl} is the relative diffraction intensity of (hkl) diffraction peak from the experimental data, I_{0hkl} is the standard peak intensity of the reflection (hkl) according to the JCPDS (Joint Committee for Powder Diffraction Studies) reference file, n is the number of diffraction peaks. For random distribution, $\mathrm{TC}_{hkl} = 1$.

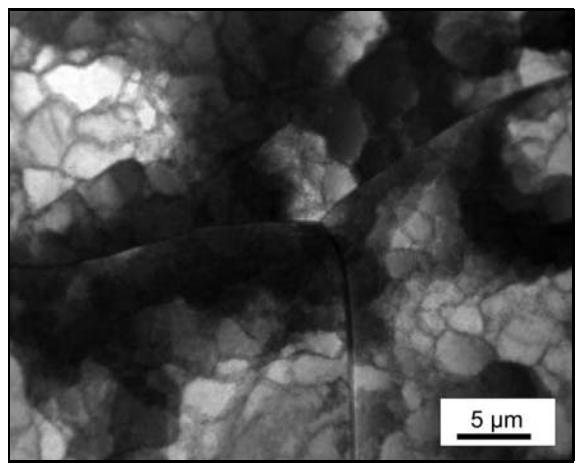

Fig. 3. TEM microstructure of pure aluminium after four ECAP passes.

3. Results and discussion

3.1. Pure aluminium

3.1.1. Microstructure

The microstructure evolution during the ECAP process was examined by TEM. TEM microstructure of the as-received pure aluminium, Fig. 1, shows that any grains interior can be almost free from dislocations (it contains only a few dislocations lines waved but not tangled together) or separated into cells with size $\sim 3\,\mu\mathrm{m}$. After the second ECAP pass a significant accumulation of tangled dislocations in individual grains in comparison with the as-received microstructure is observed, Fig. 2. After the fourth ECAP pass a marked refinement of the microstructure in complete volume into the cell/subgrain array is observed, Fig. 3. Cells/subgrains are ultrafine, almost equiaxed. The mean cell/subgrain size is $1.7\,\mu\mathrm{m}$. The detailed view of the microstructure after the fourth ECAP

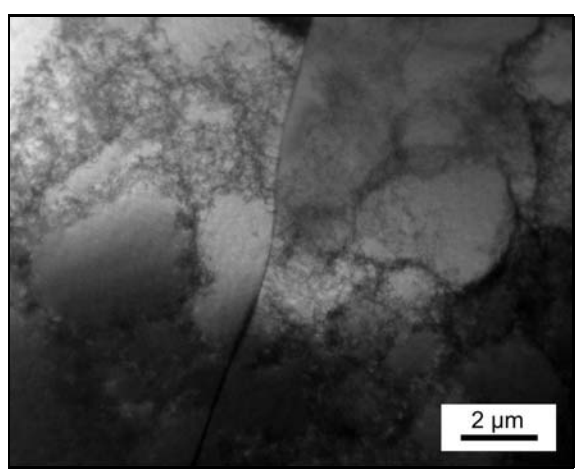

Fig. 4. Higher magnification of typical microstructure in pure aluminium after four ECAP passes.

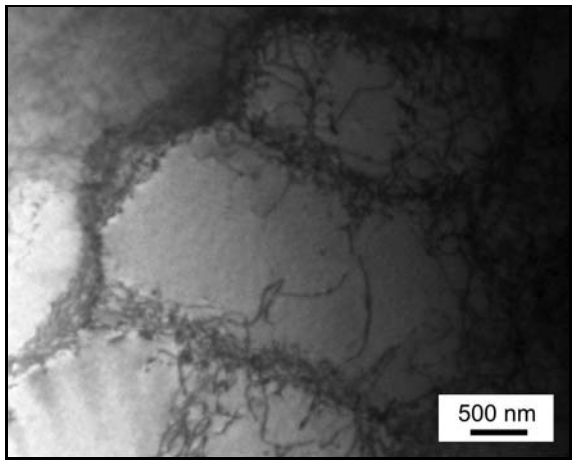

Fig. 5. TEM microstructure of pure aluminium after six ECAP passes.

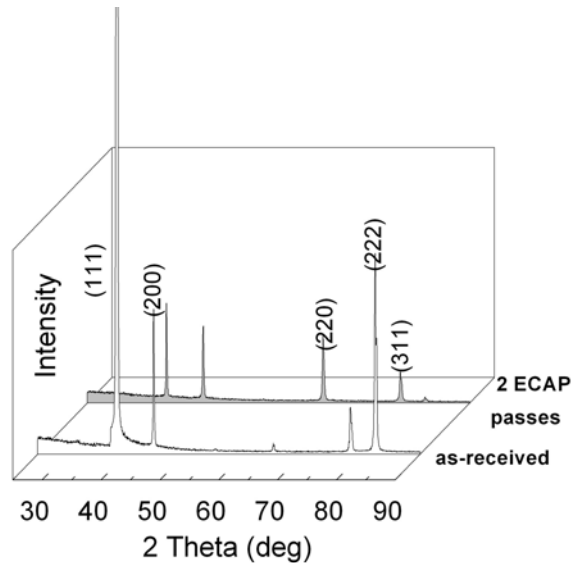

Fig. 6. XRD patterns of as-received pure aluminium and after two ECAP passes.

pass at higher magnification is in Fig. 4. This figure documents chaotic networks of the dislocations in some regions of the microstructure. There are many dislocations apparent both within the subgrains and along the subgrain boundaries. Heterogeneity of the dislocations distribution can originate in inhomogeneous straining, i.e., different regions of the grain cross over the different strains during the deformation. Considering a very low value of the dislocation density in the as-received aluminium it can be concluded that during the high deformation the multiplication of dislocation is done, which results in an increase of the dislocation density. The dislocation generation was probably accelerated due to the accumulation of the density caused by the dislocation storage. After the six ECAP passes the microstructure remained ultrafine subgrained and was practically unchanged in comparison with the microstructure after four ECAP passes. Detailed view of the microstructure after six ECAP passes is in Fig. 5. In general, according to the equivalent strain accumulation formula [29], the value of accumulated strain in the material during the ECAP process increased with the increasing number of passes which would result in better effect on the structure refinement. The unincreased value of the dislocation density observed on TEM in our material after the sixth ECAP pass, Fig. 5, in comparison with the material after the fourth ECAP pass, Fig. 4, can be a result of the balanced dislocation creation and their annihilation. Additional reason can follow that a metal with the fcc lattice is characterized by more slip planes. The aluminium is characterized by high stacking fault energy, in which a cross slip occurs very easily and thus, during the following steps of the deformation, dislocations can move easily towards the grain boundaries. Any dislocation can be absorbed into the grain boundaries. The conditions of the deformation during the refinement and structure development process play an important role [30]. Our experiments confirmed that materials processed by route C still generally contained a large fraction of subgrains [31]. The applied ECAP by route C which is 180° rotation of the billet, giving a direct reversal of the strain path each alternate cycle, leads to a consistently lower rate of grain refinement compared to the deformation without a change in strain path under a wide range of conditions [31]. From the microstructural analyses it results that the initial grain/subgrain shape remains well preserved after every even pass. It is due to the route C of ECAP, a specific strain path during which strain reversal took place between subsequent passes so that the straining direction was reversed. According to this, the recovery of the grain shape to the initial state is expected every second pass [32, 33].

3.1.2. Texture

The XRD spectrum of the as-received pure aluminium sample is shown in Fig. 6. The obtained reflexes belong to (111), (200), (220), (311) and (222) planes of the aluminium (reference code: 04-0787). The measured relative intensities of the individual aluminium diffraction peaks in this figure are not identical with the relative intensities of the aluminium standard, and this indicates that the as-received aluminium is characterized by preferred crystallographic orientation**.** The calculated values of the TCs are presented in Table 1. For a preferentially oriented sample, the texture coefficient $TC_{(hkl)}$ should be greater than one. Accordingly the as-received pure aluminium material is characterized with relatively sharp texturing for (200) planes.

Table 1. Texture coefficients of the as-received and ECAP deformed pure aluminium

hkl	Pure Al			
	TC			
	As-received	ECAP passes		
		2	4	6
111	0.99	0.38	0.33	0.35
200	1.53	2.66	2.20	2.22
220	0.17	0.46	0.46	0.47
311	1.07	1.31	1.70	1.45
222	1.24	0.31	0.33	0.47

The XRD spectrum of the pure aluminium sample after 2 passes of the ECAP compared with the XRD spectrum of the as-received specimen is documented in Fig. 6. The intensity changes of the individual aluminium reflections after the second ECAP pass in comparison with the as-received sample are evident. The intensities of (111) and (222) planes decreased significantly. In shear deformation of aluminium and aluminium alloys an activation of the main ideal shear plane (111) is normal [22, 34]. The plane (222) is the secondary reflection slip plane of (111). Next slip planes easily rotate and incline during the ECAP process, what is in agreement with our observations. The calculated values of the TCs (from Fig. 6) for pure aluminium material after 2 ECAP passes are documented in Table 1. The pure aluminium after the second ECAP pass is characterized by two dominating crystal orientations. A high value of $TC_{(200)}$ after the second ECAP pass (almost twice higher in comparison with the starting state) indicates the presence of similar but markedly stronger than as-received texturing for Al (200) planes. The material after the second ECAP pass shows texturing for Al (311) planes, too. This texture keeps the maintenance during the subsequent 4 and 6 of the ECAP passes, Table 1.

Large plastic strains during the ECAP process involved changes in the orientation distribution of crystals that composed a polycrystal, and the ECAP was associated with the development of the marked crystallographic texture. The crystallographic texture after each even pass was the shear texture.

3.2. Dispersion strengthened Al-4vol.%Al_4C_3 system

3.2.1. Microstructure

The typical TEM micrograph of the as-received Al-4vol.%Al_4C_3 composite in the radial direction is given in Fig. 7. The microstructure consists mainly from the fine grains elongated parallel to the extrusion direction. The mean grain diameter that was measured vertically on the extrusion direction is 0.5 μm (ranged from 0.3 to 0.7 μm). The Al_4C_3 second-phase particles are placed in the parallel rows as a result of the extrusion. They are lying both within the grains and on some grain boundaries. Inside many grains, the dislocations are fixed in the secondary phase particles and create a dislocation network. Morphologically, the Al_4C_3 particles are elongated but they have only a low aspect ratio, therefore they can be approximated as spherical. The Al_4C_3 particles in these materials can be divided into two dimensional groups: A – very fine particles with mean diameter size approximately 30 nm, and B – large particles with mean size around 1 μm.

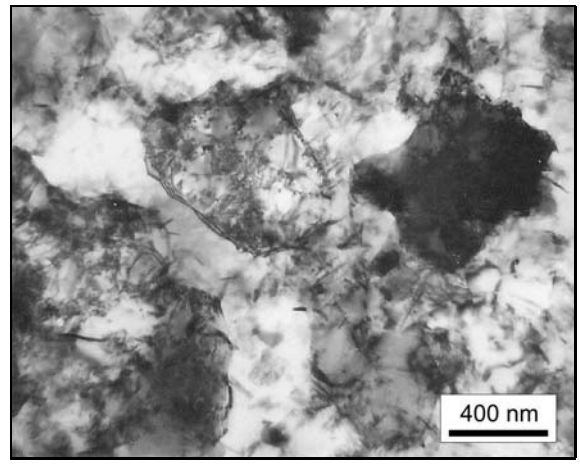

Fig. 7. TEM microstructure of as-received Al-4vol.%Al_4C_3 powder alloy.

In our previous report [35], there is a detailed microstructural analysis of the aluminium alloys. The presence of approximately 1 vol.% Al_2O_3 particles was documented in the examined system. The Al_2O_3 phase represents coarser particles with size around 0.5 μm approximately of spherical morphology. It was found that the coarse micrometer-scale particles accelerated the rate of grain refinement by generating new high angle boundaries within their deformation zone. Nanometer scale dispersoids located at the grain boundaries stabilize the boundaries and can retard the rate of grain refinement by homogenizing the slip [36].

Figure 8 shows the microstructure after processing by two ECAP passes observed by TEM. The Al_4C_3 particles were not sheared during the deformation, they were uniformly distributed within the metallic matrix and they did not change their initial shape and size during the high strain deformation. The microstructure of DS material after the second pass consisted from the equiaxed mainly nano-dimensional

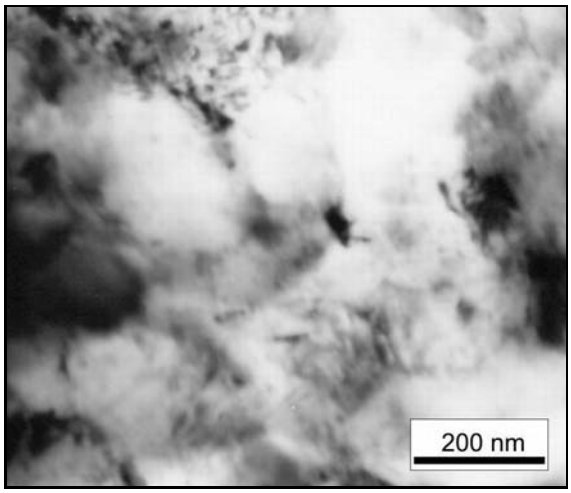

Fig. 8. TEM microstructure of Al-4vol.%Al_4C_3 powder alloy after two ECAP passes.

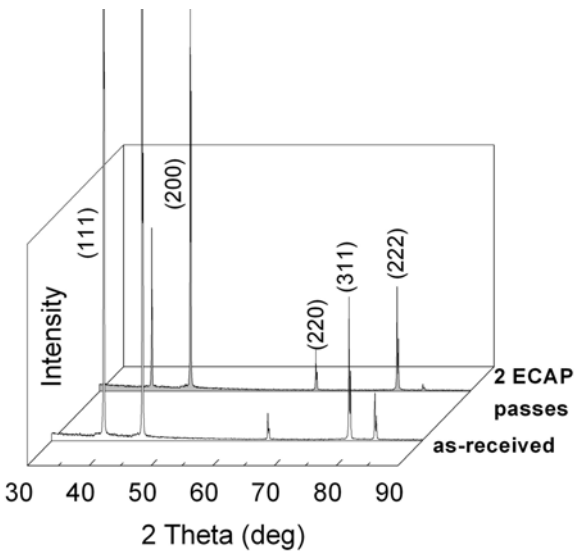

Fig. 9. XRD patterns of as-received Al-4vol.%Al_4C_3 powder alloy after two ECAP passes.

grains. The size of the grains was approximately 100 nm.

The ECAP pressing led to the transversal fragmentation of the as-received elongated grains and more isotropic microstructure. The dislocation density was high. The dislocations were present in the grains, too, but mostly on the boundaries, weakly visible due to the tilted specimen. During the deformation, gliding dislocations can by-pass small dispersoids that intersect their slip plane by the Orowan mechanism, or by cross slip, or prismatic loops, and this will greatly increase the dislocation density compared with a single phased alloy [37]. The nanostructure formation most probably includes creation of cell structure, then formation of unstable cell nanostructure with large angle disorientation and subsequent formation of nanometric grains (grain size – 100 nm) [38].

It was not possible to expose this material to the next deformation after the second ECAP pass, because the material achieved limiting state (the plasticity had zero value due to the condition of the microstructure).

Table 2. Texture coefficients of the as-received and ECAP deformed Al-4vol.%Al_4C_3 alloy

hkl	Al-4vol.%Al_4C_3	
	TC	
	As-received	2 ECAP passes
111	0.22	0.52
200	0.65	0.95
220	2.59	2.1
311	0.73	0.95
222	0.24	0.48

3.2.2. Texture

The XRD pattern of the as-received Al-4vol.% Al_4C_3 material (in the radial direction) is shown in Fig. 9. The shown reflexes belong to the (111), (200), (220), (311) and (222) planes of the aluminium (reference code: 04-0787). The presence of the Al_4C_3 phase was not recorded in this experimental material. This could be caused by the low amount of the present Al_4C_3 phase (non-detected by X-ray analysis), and simultaneously by the homogeneous distribution of the very fine Al_4C_3 particles in the Al matrix. Calculated values of the TCs (from Fig. 9) are documented in Table 2. The as-received DS aluminium is characterized by strong texturing for (111) planes considering the $TC_{(111)}$ and $TC_{(222)}$ are much greater than one. This dominating crystal orientation is characteristic for the present extruded material [39].

The XRD pattern of the DS material after the second ECAP pass in comparison with as-received material is presented in Fig. 9. The visible intensity changes indicate the texture change during the ECAP deformation. From the calculated values of the TCs, Table 2, it can be resulted that the initial dominating crystal orientation Al (111) evolved during the ECAP to strong Al (220) orientation. In comparison with common, in ECAP investigated alloys, the present alloy is characterized by very small initial grain size and high strength. The amount of rotated grains during the intensive shear deformation increased with increasing flow shear strength on crystallographic slip systems and with decreasing grain size [19]. Hence, in this DS material grain rotation was promoted and the

shear component {111} was clearly activated during the ECAP process.

From realized measurements and obtained results it can be concluded that the identical feature of both materials is the activation of the ideal shear planes, main shear plane (111) and its multiple (222) plane during the ECAP process. The texture evolution in material during the ECAP strongly depends on the initial material conditions, composition and texture.

3. Conclusions

The microstructure of the high purity aluminium and DS Al-4vol.%Al_4C_3 alloys evolved during the ECAP deformation in different ways. The microstructure evolution of the pure aluminium consisted of the creation of the dislocation cell structure, followed by the subgrain boundaries formation. In the DS material the transversal fragmentation of the elongated grains and formation of nanostructured grains took place. The presence of dispersoid inhibits the development of new high-angle grain boundaries and the formation of the fine grain microstructure. The grain refinement in the DS system is much more effective in comparison with the pure aluminium.

The ECAP process led to the formation of the strong texture by activation of the ideal shear planes (111) in both aluminium materials. In the pure aluminium during the ECAP pressing, the as-received dominating crystal orientation Al (200) markedly sharpened with the occurrence of the second dominating crystal orientation Al (311). This texture has a tendency to be preserved in the following cycles. In DS aluminium, the change of the as-received texture Al (111) to the strong clearly defined texturing for (220) plane occurred.

Acknowledgement

The work was supported by the Slovak National Grant Agency under the VEGA projects 2/0167/10, 2/0025/11, 2/0115/12 and 1/0359/11.

References

[1] Suryanarayana, C.: Bull Mater. Sci., *17*, 1994, p. 307. doi:10.1007/BF02745220
[2] Gleiter, H.: Acta Materialia, *48*, 2000, p. 1. doi:10.1016/S1359-6454(99)00285-2
[3] Sanders, P. G., Fougere, G. E., Thompson, L. J., Eastman, J. A., Wertman, J. R.: Nanostruct. Mater., *8*, 1997, p. 243. doi:10.1016/S0965-9773(97)00167-0
[4] Valiev, R. Z., Langdom, T. G.: Rev. Adv. Mater. Sci., *13*, 2006, p. 15.
[5] Koch, C. C.: Nanostruct. Mater., *9*, 1997, p. 13. doi:10.1016/S0965-9773(97)00014-7
[6] Valiev, R. Z., Islamgaliev, R. K., Alexandrov, I. V.: Prog. Mater. Sci., *45*, 2000, p. 103. doi:10.1016/S0079-6425(99)00007-9
[7] Iwahashi, Y., Wang, J., Horita, Z., Nemoto, M., Langdom, T. G.: Scr. Mater., *35*, 1996, p. 143. doi:10.1016/1359-6462(96)00107-8
[8] Xu, C., Furukawa, M., Horita, Z., Langdon, T. G.: Mater. Sci. Eng., *A398*, 2005, p. 66. doi:10.1016/j.msea.2005.03.083
[9] Langdon, T. G., Furukawa, M., Nemoto, M., Horita, Z.: JOM, *52*, 2000, p. 30. doi:10.1007/s11837-000-0128-7
[10] Segal, V.: Mater. Sci. Eng., *A197*, 1995, p. 157. doi:10.1016/0921-5093(95)09705-8
[11] Skrotzki, W. et al.: Acta Materialia, *55*, 2007, p. 2013. doi:10.1016/j.actamat.2006.11.005
[12] Valiev, R. Z., Langdon, T. G.: Rev. Adv. Mater. Sci., *13*, 2006, p. 15.
[13] Zrník, J., Dobatkin, V., Mamuzič, I.: Metallurgija, *47*, 2008, p. 211.
[14] Salem, A. A., Langdon, T. G., McNelley, T. R., Kalidindi, S. R., Semiatin, S. L.: Metall. Mater. Trans., *37A*, 2006, p. 2879. doi:10.1007/BF02586120
[15] Kawasaki, M., Horita, Z., Langdon, T. G.: Mater. Sci. Eng., *A 524*, 2009, p. 143. doi:10.1016/j.msea.2009.06.032
[16] Starink, M. J., Qiao, X. G., Zhang, J., Gao, N.: Acta Materialia, *57*, 2009, p. 5796. doi:10.1016/j.actamat.2009.08.006
[17] Kawasaki, M., Sklenička, V., Langdon, T. G.: Kovove Mater., *49*, 2011, p. 75. doi:10.4149/km_2011_1_75
[18] Alexandrov, I. V., Zhilina, M. V., Bonarski, J. T.: Bulletin of the Polish Academy of Sciences, *54*, 2006, p. 2.
[19] Li, S., Beyerlein, I. J., Alexander, D. J., Vogel, S. C.: Acta Mater., *53*, 2005, p. 2111. doi:10.1016/j.actamat.2005.01.023
[20] Li, S., Beyerlein, I. J., Necker, C. T., Alexander, D. J., Bourke, M.: Acta Mater., *54*, 2006, p. 1397. doi:10.1016/j.actamat.2005.11.020
[21] Zhilyaev, A. P., Oh-ishi, K., Raab, G. I., McNelley, T. R.: Mater. Sci. Eng., *A 441*, 2006, p. 245. doi:10.1016/j.msea.2006.08.029
[22] Zhu, Y. T., Lowe, T. C.: Mater. Sci. Eng., *A 291*, 2000, p. 46. doi:10.1016/S0921-5093(00)00978-3
[23] Berbon, P. B., Furukawa, M., Horita, Z., Nemoto, M., Langdon, T. G.: Metal Mater. Trans., *30A*, 1999, p. 1989.
[24] Wang, S. C., Starink, M. J., Gao, N., Qiao, X. G., Xu, C., Langdon, T. G.: Acta Mater., *56*, 2008, p. 3800. doi:10.1016/j.actamat.2008.04.022
[25] Varchola, M., Besterci, M., Sülleiová, K.: Materials Engineering, *16*, 2009, p. 1.
[26] Kvačkaj, T., Besterci, M., Ballóková, B.: Acta Metallurgica Slovaca, *10*, 2004, p. 5.
[27] Alexandrov, I. V. M., Zhilina, V., Bonarski, J. T.: Bulletin of the Polish Academy of Sciences, Technical Sciences, *54/2*, 2006, p. 99.
[28] Barrett, C. S., Massalski, T. B.: Structure of Metals. Oxford, Pergamon 1980.
[29] Sun, P. L., Yu, C. Y., Kao, P. W., Chang, C. P.: Scripta Mater., *47*, 2002, p. 377. doi:10.1016/S1359-6462(02)00117-3

[30] Lewandowska, M., Garbacz, H., Pachla, W., Mazur, A., Kurzydlowski, K. J.: Materials Science-Poland, *23*, 2005, p. 279.
[31] Prangnell, P. B., Bowen, J. R., Gholinia, A.: In: Proceedings of the 22nd Riso International Symposium on Material Science, Denmark 2001.
[32] Gu, C. F., Tóth, L. S.: Acta Materialia, *59*, 2011, p. 5749. doi:10.1016/j.actamat.2011.05.051
[33] Gu, C. F., Tóth, L. S., Davies, C. H. J.: Scripta Mater., *65*, 2011, p. 167. doi:10.1016/j.scriptamat.2011.04.009
[34] Cao, W. Q., Godfrey, A., Liu, Q.: Mat. Sci. Eng., *A 361*, 2003, p. 9. doi:10.1016/S0921-5093(03)00055-8
[35] Berta, M., Apps, P., Prangnell, P. B.: Materials Science and Engineering, *A 410*, 2005, p. 411. doi:10.1016/j.msea.2005.08.026
[36] Ďurišinová, K., Ďurišin, J., Orolínová, M., Ďurišin, M.: J. Alloys Compd., *525*, 2012, p. 137. doi:10.1016/j.jallcom.2012.02.098
[37] Apps, P. J., Berta, M., Prangnell, P. B.: Acta Mater., *53*, 2004, p. 49.
[38] Besterci, M., Velgosová, O., Ivan, J., Kvačkaj, T.: Kovove Mater., *47*, 2009, p. 221.
[39] Ďurišin, J., Orolínová, M., Ďurišinová, K., Besterci, M.: Kovove Mater., *45*, 2007, p. 269.